

# Unsupervised Data Uncertainty Learning in Visual Retrieval Systems

Ahmed Taha<sup>1</sup> Yi-Ting Chen<sup>2</sup> Teruhisa Misu<sup>2</sup> Abhinav Shrivastava<sup>1</sup> Larry Davis<sup>1</sup>

## Abstract

We introduce an unsupervised formulation to estimate heteroscedastic uncertainty in retrieval systems. We propose an extension to triplet loss that models data uncertainty for each input. Besides improving performance, our formulation models local noise in the embedding space. It quantifies input uncertainty and thus enhances interpretability of the system. This helps identify noisy observations in query and search databases. Evaluation on both image and video retrieval applications highlight the utility of our approach. We highlight our efficiency in modeling local noise using two real-world datasets: Clothing1M and Honda Driving datasets. Qualitative results illustrate our ability in identifying confusing scenarios in various domains. Uncertainty learning also enables data cleaning by detecting noisy training labels.

## 1. Introduction

Noisy observations hinder learning from supervised datasets. Adding more labeled data does not eliminate this inherent source of uncertainty. For example, object boundaries and objects farther from the camera remain challenging in semantic segmentation, even for humans. Noisy observations take various forms in visual retrieval. The noise can be introduced by a variety of factors; e.g., low resolution inputs, a wrong training label. Modeling uncertainty in training data can improve both the robustness and interpretability of a system. In this paper, we propose a formulation to capture data uncertainty in retrieval applications. Figure 1 shows the lowest and highest uncertainty query images, detected by our system, from DukeMTMC-ReID person re-identification dataset. Similarly, in autonomous navigation scenarios, our formulation can identify confusing scenarios; thus improving the retrieval efficiency and interpretability in this safety-critical system.

Labeled datasets contain observational noise that corrupts

<sup>1</sup>Univeristy of Maryland, College Park <sup>2</sup>Honda Research Institute, USA. Correspondence to: Ahmed Taha <ahmd-taha@cs.umd.edu>.



Figure 1: The first and second rows show five lowest and highest uncertainty queries (respectively) identified from DukeMTMC-ReID dataset.

the target values (Bishop et al., 1995). This noise, also known as aleatoric uncertainty (Kendall & Gal, 2017), is inherent in the data observations and cannot be reduced even if more data is collected. Aleatoric uncertainty is categorized into homoscedastic and heteroscedastic uncertainty. Homoscedastic uncertainty is task dependent, i.e., a constant observation noise  $\sigma$  for all input points. On the contrary, heteroscedastic uncertainty posits the observation noise  $\sigma(x)$  as dependent on input  $x$ . Aleatoric uncertainty has been modeled in regression and classification applications like per-pixel depth regression and semantic segmentation tasks respectively. In this paper, we extend triplet loss formulation to model heteroscedastic uncertainty in retrieval applications.

Triplet loss (Schroff et al., 2015) is a prominent ranking loss for space embedding. It has been successfully applied in face recognition (Schroff et al., 2015; Sankaranarayanan et al., 2016) and person re-identification (Cheng et al., 2016; Su et al., 2016; Ristani & Tomasi, 2018). In this paper, we extend it to capture heteroscedastic uncertainty in an unsupervised manner. Vanilla triplet loss assumes a constant uncertainty for all input values. By integrating the anchor, positive, and negative uncertainties ( $\sigma_a$ ,  $\sigma_p$ , and  $\sigma_n$  respectively) in the loss function, our model learns data uncertainty nonparametrically. Thus, the data uncertainty becomes a function of different inputs, i.e., every object has a different  $\sigma(x)$ .

We evaluate our unsupervised formulation on two image retrieval applications: person re-identification and fashion item retrieval. Person re-identification datasets provide an established quantitative evaluation benchmark. Yet, they have little emphasis on confusing samples. Thus, we leverage Clothing1M (Xiao et al., 2015) fashion classification dataset for its noisy labels and inter-class similarities. The training split has a small clean and a large noisy labeled subsets. Inter-class similarity, *e.g.*, *Down Coat* and *Wind-breaker*, and images with wrong labels are two distinct confusion sources, both of which are captured by our learned uncertainty model.

One of the main objectives behind modeling uncertainty is improving safety, since uncertainty quantification can prevent error propagation (McAllister et al., 2017). To this end, we employ Honda driving dataset (HDD) (Ramanishka et al., 2018) for evaluation on safety-critical autonomous navigation domain. Explicit heteroscedastic uncertainty representation improves retrieval performance by reducing the effect of noisy data with the implied attenuation. Qualitative evaluation demonstrates the ability of our approach to identify confusing driving situations.

In summary, the key contributions of this paper are:

1. Formulating an unsupervised triplet loss extension to capture heteroscedastic (data) uncertainty in visual retrieval systems.
2. Improving retrieval model’s interpretability by identifying confusing visual objects in train and test data. This reduces error propagation and enables data cleaning.
3. Harnessing heteroscedastic uncertainty to improve efficiency by 1-2% and improving model stability by modeling local noise in the embedding space.

## 2. Related Work

### 2.1. Bayesian Uncertainty Modeling

Bayesian models define two types of uncertainty: epistemic and aleatoric. Epistemic uncertainty, also known as model uncertainty, captures uncertainty in model parameters. It reflects generalization error and can be reduced given enough training data. Aleatoric uncertainty is the uncertainty in our data, *e.g.*, uncertainty due to observation noise. Kendall and Gal (2017) divide it into two sub-categories: heteroscedastic and homoscedastic. Homoscedastic is task-dependent uncertainty not dependent on the input space, *i.e.*, constant for all input data and varies between different tasks. Heteroscedastic varies across the input space due to observational noise, *i.e.*,  $\sigma(x)$ .

Quantifying uncertainties can potentially improve the performance, robustness, and interpretability of a system. Therefore, epistemic uncertainty modeling has been leveraged for semantic segmentation (Nair et al., 2018), depth esti-

mation (Kendall & Gal, 2017), active learning (Gal et al., 2017), conditional retrieval (Taha et al., 2019), and model selection (Gal & Ghahramani, 2016) though hyper-parameter tuning. A supervised approach to learning heteroscedastic uncertainty to capture observational noise has been proposed (Nix & Weigend, 1994; Le et al., 2005). However, labeling heteroscedastic uncertainty in real-world problems is challenging and not scalable.

A recent approach (Kendall & Gal, 2017) regresses this uncertainty without supervision. This approach has been applied in semantic segmentation and depth estimation. By making the observation noise parameter  $\sigma$  data-dependent, it can be learned as a function of the data  $x_i$  as follows

$$L = \frac{1}{N} \sum_{i=1}^N \frac{1}{2\sigma(x_i)^2} \|y_i - f(x_i)\|^2 + \frac{1}{2} \log \sigma(x_i), \quad (1)$$

for a labeled dataset with  $N$  points of  $(x_i, y_i)$  and  $f(x_i)$  is a uni-variate regression function. This formulation allows the network to reduce the erroneous labels’ effect. The noisy data with predicted high uncertainty will have a smaller effect on the loss function  $L$  which increases the model robustness. The two terms in equation 1 have contradicting objectives. While the first term favors high uncertainty for all points, the second term  $\log(\sigma(x_i))$  penalizes it.

We extend triplet loss to learn data uncertainty in a similar unsupervised manner. The network learns to ignore parts of the input space if uncertainty justifies penalization. This form of learned attenuation is a consequence of the probabilistic interpretation of (Kendall & Gal, 2017) model.

### 2.2. Triplet Loss

To learn a space embedding, we leverage triplet loss for its simplicity and efficiency. It is more efficient than contrastive loss (Hadsell et al., 2006; Li et al., 2017), and less computationally expensive than quadruplet (Huang et al., 2016b; Chen et al., 2017) and quintuplet (Huang et al., 2016a) losses. Equation 2 shows the triplet loss formulation

$$L_{\text{tri}} = \frac{1}{b} \sum_{i=1}^b [(D([a], [p]) - D([a], [n]) + m)]_+, \quad (2)$$

where  $[\cdot]_+$  is a soft margin function and  $m$  is the margin between different classes embedding.  $[\cdot]$  and  $D(\cdot, \cdot)$  are the embedding and the Euclidean distance functions respectively. This formulation attracts an anchor image  $a$  of a specific class closer to all other positive images  $p$  from the same class than it is to any negative image  $n$  of other classes.

The performance of triplet loss relies heavily on the sampling strategy used during training. We experiment with both hard (Hermans et al., 2017) and semi-hard sampling (Schroff et al., 2015) strategies. In semi-hard negative

sampling, instead of picking the hardest positive-negative samples, all anchor-positive pairs and their corresponding semi-hard negatives are considered. Semi-hard negatives are further away from the anchor than the positive exemplar, yet within the banned margin  $m$ . Figure 2 shows a triplet loss tuple and highlights different types of negative exemplars. Hard and semi-hard negatives satisfy equations 4 and 3 respectively.

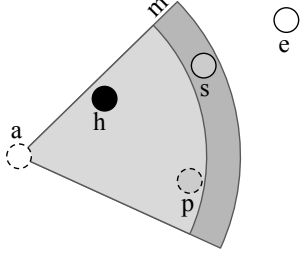


Figure 2: Triplet loss tuple (anchor, positive, negative) and margin  $m$ . (H)ard, (s)emi-hard and (e)asy negatives highlighted in black, gray and white respectively.

$$D([a], [p]) < D([a], [n]) < D([a], [p]) + m, \quad (3)$$

$$p = \operatorname{argmax}_i D([a], [i]), n = \operatorname{argmin}_i D([a], [i]). \quad (4)$$

Triplet loss has been extended to explore epistemic (model) uncertainty (Taha et al., 2019). In this paper, we propose a similar formulation to learn heteroscedastic (data) uncertainty.

### 2.3. Bayesian Retrieval

Dropout as a Bayesian approximation framework has been theoretically studied for both classification and regression problems (Gal & Ghahramani, 2016; Kendall & Gal, 2017). To extend this framework to retrieval and space embedding problems, triplet loss is cast as a regression function (Taha et al., 2019). Given a training dataset containing  $N$  triplets  $\{(x_1, y_1, z_1), (x_2, y_2, z_2), \dots, (x_n, y_n, z_n)\}$  and their corresponding outputs  $(d_1, \dots, d_n)$ , the triplet loss can be formulated as a trivariate regression function as follows

$$f_{\text{tri}}(x_i, y_i, z_i) = d_i \in [0, 2 + m] \quad (5)$$

$$= [D([x_i], [y_i]) - D([x_i], [z_i]) + m]_+. \quad (6)$$

Assuming a unit-circle normalized embedding,  $f_{\text{tri}}(x_i, y_i, z_i)$  outputs  $d_i = 0$  if  $y_i, x_i \in c_i$  and  $z_i \in c_j$ ; and  $d_i = 2 + m$  if  $z_i, x_i \in c_i$  and  $y_i \in c_j$  s.t.  $i \neq j$ . This casting enables epistemic uncertainty learning for multi-modal conditional retrieval systems (Taha et al., 2019). Inspired by this, Section 3 presents our proposed extension to capture heteroscedastic uncertainty.

## 3. Heteroscedastic Embedding

Heteroscedastic models investigate the observation space and identify parts suffering from high noise levels. Taha et al. (2019) cast normalized ranking losses as a regression function to study epistemic uncertainty. Similarly, we extend triplet loss to learn the data-dependent heteroscedastic uncertainty. This helps identify noisy and confusing objects in a retrieval system, either in queries or in the search gallery.

Normalized triplet loss is cast as a trivariate regression function (Taha et al., 2019). It is straight-forward to extend it for unnormalized embedding with soft margin as follows

$$f_{\text{tri}}(x_i, y_i, z_i) = d_i \in [0, \infty) \quad (7)$$

$$= [D([x_i], [y_i]) - D([x_i], [z_i])]_+. \quad (8)$$

$f_{\text{tri}}(x_i, y_i, z_i)$  outputs  $d_i = 0$  if  $y_i, x_i \in c_i$  and  $z_i \in c_j$ ; and  $d_i \rightarrow \infty$  if  $z_i, x_i \in c_i$  and  $y_i \in c_j$  s.t.  $i \neq j$ . Unlike the univariate regression formulation (Kendall & Gal, 2017), triplet loss is dependent on three objects: anchor, positive, and negative. We extend the vanilla triplet loss to learn a noise parameter  $\sigma$  for each object independently, i.e.,  $\sigma_a, \sigma_p, \sigma_n$ . For a single triplet  $(a, p, n)$ , the vanilla triplet loss is evaluated three times as follows

$$\begin{aligned} f_{\text{tri}}(a, p, n) &= \frac{1}{2\sigma_a^2} L_{\text{tri}}(a, p, n) + \frac{1}{2} \log \sigma_a^2 \\ &+ \frac{1}{2\sigma_p^2} L_{\text{tri}}(a, p, n) + \frac{1}{2} \log \sigma_p^2 \\ &+ \frac{1}{2\sigma_n^2} L_{\text{tri}}(a, p, n) + \frac{1}{2} \log \sigma_n^2 \quad (9) \\ &= \frac{L_{\text{tri}}(a, p, n)}{2} \left( \frac{1}{\sigma_a^2} + \frac{1}{\sigma_p^2} + \frac{1}{\sigma_n^2} \right) \\ &+ \frac{1}{2} \log \sigma_a^2 \sigma_p^2 \sigma_n^2, \quad (10) \end{aligned}$$

where  $L_{\text{tri}}(a, p, n) = [D([a], [p]) - D([a], [n])]_+$ . This formulation can be regarded as a weighted average triplet loss using data uncertainty. Similar to (Kendall & Gal, 2017), we compute a maximum a posteriori probability (MAP) estimate by adding a weight decay term parameterized by  $\lambda$ . This imposes a prior on the model parameters and reduces overfitting (Le et al., 2005). Our neural network learns  $s = \log \sigma^2$  because it is more numerically stable than regressing the variance  $\sigma^2$ . Thus, in practice the final loss function is

$$\begin{aligned} L &= \frac{1}{N} \sum_{(a,p,n) \in \mathcal{T}} \left[ \frac{(e^{-s_a} + e^{-s_p} + e^{-s_n}) L_{\text{Tri}}(a, p, n)}{2} \right. \\ &\quad \left. + \frac{(s_a + s_p + s_n)}{2} \right] + \lambda \|W\|^2, \quad (11) \end{aligned}$$

where  $N$  is the number of triplets  $(a, p, n) \in \mathcal{T}$ . Our formulation can be generalized to support more complex ranking

losses like quintuplet loss (Huang et al., 2016a). Equation 12 provides a generalization for k-tuplets where  $k \geq 3$

$$f_{k\_tup}(x_0, \dots, x_j, \dots, x_k) = \frac{L_{tri}(a, p, n)}{2} \left( \sum_{j=0}^k \frac{1}{\sigma_j^2} \right) + \frac{1}{2} \log \prod_{j=0}^k \frac{1}{\sigma_j^2} \quad (12)$$

$$\text{s.t. } D(\lfloor x_0 \rfloor, \lfloor x_1 \rfloor) < D(\lfloor x_0 \rfloor, \lfloor x_j \rfloor) < D(\lfloor x_0 \rfloor, \lfloor x_k \rfloor). \quad (13)$$

## 4. Architecture

The generic architecture employed in our experiments is illustrated in Figure 3. The encoder architecture is dependent on the input type. For an embedding space with dimensionality  $d$ , our formulation requires the encoder final layer output  $\in R^{d+1}$ . The extra dimension learns the input heteroscedastic uncertainty  $\sigma(x)$ . The following subsections present two encoder variants employed to properly handle image and video inputs.

### 4.1. Image Retrieval

For image-based tasks of person re-identification and fashion item retrieval, we employ the architecture from (Hermans et al., 2017). Given an input RGB image, the encoder is a fine-tuned ResNet architecture (He et al., 2016) pretrained on ImageNet (Deng et al., 2009) followed by a fully-connected network (FCN). In our experiments, the final output is not normalized and the soft margin between classes is imposed by the softplus function  $\ln(1 + \exp(\bullet))$ . It is similar to the hinge function  $\max(\bullet, 0)$  but it decays exponentially instead of a hard cut-off. We experiment with both hard and semi-hard negative sampling strategies for person re-identification and fashion item retrieval respectively.

### 4.2. Video Retrieval

For autonomous navigation, a simplified version of (Taha et al., 2019) architecture is employed. The Honda driving dataset provides multiple input modalities, e.g., camera and CAN sensors, and similarity notions between actions (events). We employ the camera modality and two similarity notions: *goal-oriented* and *stimulus-driven*. Input video events from the camera modality are represented using pre-extracted features per frame, from the Conv2d-7b-1x1 layer of InceptionResnet-V2 (Szegedy et al., 2017) pretrained on ImageNet, to reduce GPU memory requirements.

Modeling temporal context provides an additional and important clue for action understanding (Simonyan & Zisserman, 2014). Thus, the encoder employs an LSTM (Furukawa & Nakamura, 1993; Hochreiter & Schmidhuber, 1997) after a shallow CNN. During training, three random

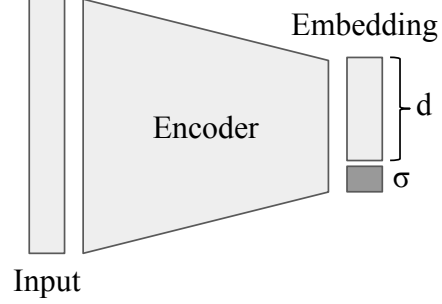


Figure 3: Our generic retrieval network supports various encoder architectures trained through a ranking loss.

consecutive frames are drawn from an event. They are independently encoded then temporally fused using the LSTM. Note that sampling more frames per event will lead to better performance. Unfortunately, the GPU memory constrains the number of sampled frames to three. The network output is the hidden state of the LSTM last time step. Further architectural details are described in the supplementary material.

## 5. Experiments

We evaluate our formulation on three retrieval domains through three datasets. First, it is validated using the standard person-identification benchmark (Zheng et al., 2017). In order to model inter-class similarity and local noise, we leverage two real-world datasets: Clothing1M and Honda Driving Dataset (HDD). Both datasets emulate real scenarios with noisy labels due to inter-class similarity or inherent uncertainty.

### 5.1. Person Re-Identification

Person re-identification is employed in Multi-Target Multi-Camera Tracking system. An ID system retrieves images of people and ranks them by decreasing similarity to a given person query image. DukeMTMC-reID (Zheng et al., 2017) is used for evaluation. It includes 1,404 identities appearing in more than two cameras and 408 identities appearing in a single camera for distraction purpose. 702 identities are reserved for training and 702 for testing. We evaluate our formulation using this clean dataset for two reasons: (1) It provides an established quantitative benchmark to emphasize the competence and robustness of our approach; (2) qualitative results comprehension requires no domain-specific knowledge.

For each training mini-batch, we uniformly sample  $P = 18$  person identities without replacement. For each person,  $K = 4$  sample images are drawn without replacement with resolution  $256 \times 128$ . The learning rate is  $3 * 10^{-4}$  for the first 15000 iterations and decays to  $10^{-7}$  at iteration 25000. Weight regularization employed with  $\lambda = 10e - 4$ .



Table 1: Quantitative evaluation on DukeMTMC-ReID

Method	mAP	Top-5
BoW+KISSME (Zheng et al., 2015)	12.17	-
LOMO+XQDA (Liao et al., 2015)	17.04	-
Baseline (Zheng et al., 2016)	44.99	-
PAN (Zheng et al., 2018)	51.51	-
SVDNet (Sun et al., 2017)	56.80	-
Tri-ResNet (Hermans et al., 2017)	<b>56.08±0.005</b>	<b>86.76±0.007</b>
<b>Tri-ResNet + Hetero (ours)</b>	55.16±0.002	86.03±0.005
Tri-ResNet + Aug	56.44±0.006	86.11±0.003
<b>Tri-ResNet + Aug + Hetero (ours)</b>	<b>56.74±0.004</b>	<b>86.20±0.002</b>

Our formulation is evaluated twice with and without data augmentation. Similar to (Ristani & Tomasi, 2018), we augment images by cropping and horizontal flipping. For illumination invariance, contrast normalization, grayscale and color multiplication effects are applied. For resolution invariance, we apply Gaussian blur of varying  $\sigma$ . For additional viewpoint/pose invariance, we apply perspective transformations and small distortions. We additionally hide small rectangular image patches to simulate occlusion.

Figure 1 shows the five lowest and highest uncertainty query-identities from the DukeMTMC-ReID dataset. Heteroscedastic uncertainty is high when the query image contains multiple identities or a single identity with an outfit that blends with the background. On the contrary, identities with discriminative outfit colors (*e.g.*, red) suffer low uncertainty.

Table 1 presents our quantitative evaluation where the performance of our method is comparable to the state-of-the-art. All experiments are executed five times, and mean average precision (mAP) and standard deviation are reported. Our formulation lags marginally due to limited confusing samples in the training split. However, it has a smaller standard deviation. It is noteworthy that the performance gap between vanilla Tri-ResNet and our formulation closes when applying augmentation. This aligns with our hypothesis that the lack of confusing samples limits our formulation. In the next subsections, we evaluate on real-world datasets containing noisy samples.

## 5.2. Fashion Image Retrieval

A major drawback of the person re-identification dataset is the absence of noisy images. Images with multiple identities are confusing but incidental in the training split. To underscore the importance of our formulation, a large dataset with noisy data is required. Clothing1M fashion dataset (Xiao et al., 2015) emulates this scenario by providing a large-scale dataset of clothing items crawled from several online shopping websites. It contains over one million images and their description. Fashion items are labeled using a noisy process: a label is assigned if the description contains the keywords of that label, otherwise, it is discarded. A small

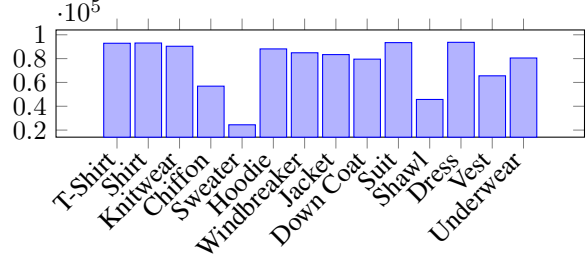


Figure 4: Clothing1M classes distribution.

Table 2: Quantitative evaluation on Clothing1M. The first row show performance with clean data only while the remaining rows leverage both clean and noisy data. The last two rows show performance after cleaning 20% of the search gallery samples

Method	mAP
Tri-ResNet (Clean Only)	52.62
Tri-ResNet (Baseline)	61.70±0.001
<b>Tri-ResNet + Hetero (ours)</b>	<b>62.27±0.001</b>
Tri-ResNet + Random Cleaning	62.33±0.003
<b>Tri-ResNet + Hetero Cleaning</b>	<b>64.57±0.002</b>

clean portion of the data is made available after manual refinement. The final training split contains 22,933 clean ( $D_c$ ) and 1,024,637 (97.81%) noisy ( $D_n$ ) labeled images. The validation and test sets have 14,313 and 10,526 clean images respectively.

Figure 4 shows the 14 classes, and their distribution, from the Clothing1M dataset. Training with both clean and noisy is significantly superior compared to just training with clean data. Since manual inspection of noisy data is expensive, our unsupervised formulation qualitatively identifies confusing samples and provides an efficient system to deal with noisy data. For clothing1M dataset, the training parameters are similar to person re-identification dataset except for the following: a minibatch has samples from all 14 classes ( $k = 10$  samples per class per minibatch) and input image resolution is  $224 \times 224$ . Semi-hard sampling strategy is employed to mitigate noisy labels effect. The model is training for 25k training iterations, which is equivalent to six epochs.

The validation and test splits act as query and gallery database respectively for quantitative evaluation. Table 2 presents retrieval performance using only clean data vs. both clean and noisy data. Mean and standard deviation across five trails are reported. By modeling data uncertainty, our formulation improves performance and interpretability of the model. We utilize the learned uncertainty to clean confusing samples from the search gallery database. The last two rows in Table 2 present retrieval performance after cleaning 20% of the search database. While random cleaning achieves no improvement, removing items suffering the



Figure 5: Qualitative evaluation using the highest five uncertainty training images from *Sweater* and *Suit* classes in Clothing1M.

highest uncertainty boosts performance by  $\sim 2\%$ .

Leveraging uncertainty to refine the training split is a plausible extension but requires extensive manual labor. Figure 5 presents the five highest uncertainty training images from two classes. The supplementary material provides a qualitative evaluation showing images with highest uncertainty score from each class. Most images are either incorrectly labeled or contain multiple distinct objects which highlights the utility of our approach.

Figure 6 depicts a negative Pearson correlation ( $r = -0.5001$ ) between the retrieval average precision of query items and their heteroscedastic uncertainty. Query images are aggregated by the average-precision percentiles on the x-axis. Aggregated items’ average uncertainty is reported on the y-axis. Figure 7 shows query images chosen from the 1<sup>st</sup> highest uncertainty percentile and their corresponding four top results. For visualization purposes, we discretize the data uncertainty using percentiles into five bins: very low (green), low (yellow), moderate (orange), high (violet), and very high (red). Confusion between certain classes like *Sweater* and *Knitwear*, *Knitwear* and *Windbreaker*, and *Jacket* and *Down coat* is evident.

Figure 8 shows a principal component analysis (PCA) 2D projection for 4K randomly chosen query items embedding. Points in the left and right projections are colored by the class label and uncertainty degree respectively. Images at the center of classes (in green) have lower uncertainty, compared to points spread out through the space. The inherent inter-class similarity, e.g., *Sweater* and *Knitwear*, explains why certain regions have very higher uncertainty. Qualitative evaluation with very low uncertainty query items is provided in the supplementary material.

### 5.3. Autonomous Navigation

Modeling network and data uncertainty is gaining momentum in safety-critical domains like autonomous driving. We evaluate our approach on ego-motion action retrieval. Honda driving dataset (HDD) (Ramanishka et al., 2018) is designed to support modeling driver behavior and under-

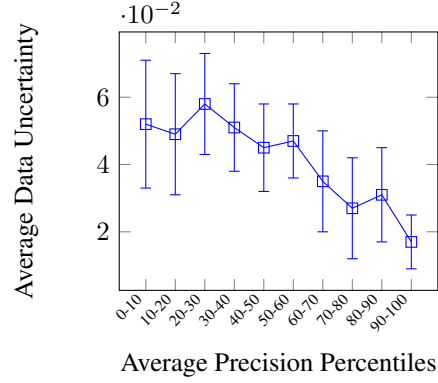


Figure 6: Quantitative analysis reveals the  $-ve$  correlation between query images retrieval average precision and uncertainty. Queries with high average precision suffer lower uncertainty and vice versa. Query images are aggregated using average precision percentiles on the x-axis. Y-axis is the aggregated images’ mean uncertainty and standard deviation.



Figure 7: Qualitative evaluation using three very high uncertainty queries from Clothing1M dataset. Outline colors emphasize the uncertainty degree, e.g., red is very high. Inter-class similarity is a primary confusion source.

standing causal reasoning. It defines four annotation layers. (1) **Goal-oriented actions** represent the egocentric activities taken to reach a destination like left and right turns. (2) **Stimulus-driven** are actions due to external causation factors like stopping to avoid a pedestrian or stopping for a traffic light. (3) **Cause** indicates the reason for an action. Finally, the (4) **attention** layer localizes the traffic participants that drivers attend to. Every layer is categorized into a set of classes (actions). Figures 9 and 10 show the class distribution for goal-oriented and stimulus-driven layers respectively.

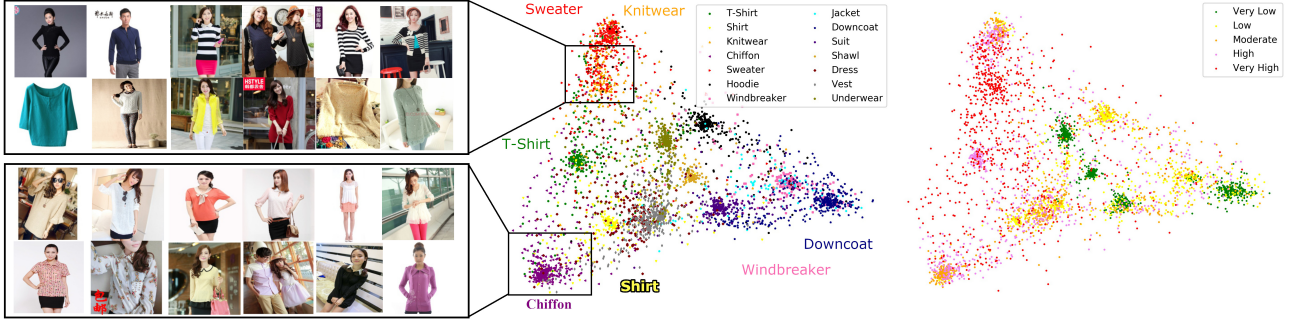


Figure 8: Qualitative analysis for the Clothing1M dataset embedding using 4K random points. The left and right plots show a 2D PCA projection colored with class-label and uncertainty degree respectively. Points closer to class centers suffer lower uncertainty compared to farther points. Confusing inter-class similarity is highlighted with visual samples. The left zoom-in figures show four rows with samples from *Sweater*, *Knitwear*, *Chiffon*, and *Shirt* respectively. These high-resolution figures are best viewed in color/screen.

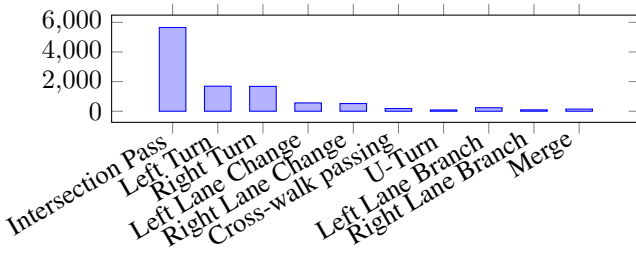


Figure 9: HDD long tail goal-oriented actions distribution.

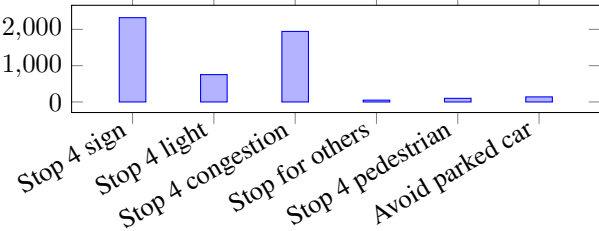


Figure 10: HDD imbalance stimulus-driven actions distribution.

Experiments’ technical details are presented in the supplementary material. An event retrieval evaluation using query-by-example is performed. Given a query event, similarity scores to all events are computed, *i.e.*, a leave-one-out cross evaluation on the test split. Performances of all queries are averaged to obtain the final evaluation.

To tackle data imbalance and highlight performance on minority classes, both micro and macro average accuracies are reported. Macro-average computes the metric for each class independently before taking the average. Micro-average is the traditional mean for all samples. Macro-average treats all classes equally while micro-averaging favors majority classes. Tables 3 and 4 show quantitative evaluation for networks trained on goal-oriented and stimulus-driven events respectively.

Table 3: Quantitative evaluation on goal-oriented actions

Method	Baseline	Hetero (Our)
Micro mAP	77.88±0.003	<b>78.45±0.004</b>
Macro mAP	<b>32.62±0.004</b>	30.8±0.004
Intersection Passing	89.1±0.006	91.44±0.002
Left turn	81.29±0.007	80.15±0.008
Right Turn	89.99±0.008	89.19±0.016
Left Lane Change	24.65±0.005	20.28±0.008
Right Lane Change	16.04±0.018	9.19±0.002
Crosswalk Passing	1.13±0.001	1.31±0.002
U-turn	3.59±0.004	2.62±0.003
Left Lane Branch	14.03±0.022	8.65±0.024
Right Lane Branch	2.15±0.001	1.48±0.011
Merge	4.26±0.005	3.62±0.006

Table 4: Quantitative evaluation on stimulus-driven actions

Method	Baseline	Hetero (Our)
Micro mAP	66.50±0.008	<b>68.20±0.008</b>
Macro mAP	35.33±0.005	<b>36.23±0.008</b>
Stop 4 Sign	87.85±0.005	89.18±0.006
Stop 4 Light	52.63±0.013	49.86±0.005
Stop 4 Congestion	63.88±0.014	67.88±0.016
Stop 4 Others	1.62±0.010	1.02±0.004
Stop 4 Pedestrian	2.72±0.007	2.56±0.002
Avoid Parked Car	3.30±0.002	6.90±0.024

Figure 11 presents a qualitative evaluation on HDD. Every two consecutive rows show a very high uncertainty query event and its nearest retrieval result. All query events are chosen within the 1<sup>st</sup> highest uncertainty percentile. A description containing the event class and its uncertainty degree is provided below each event. The first query (first row) shows the driver moving from the wrong direction lane to the correct one behind a pickup truck, with a huge cat drawn on a building wall. This example illustrates how uncertainty grounding is challenging in video events. The nearest event to this query (second row) is a very high uncertainty right turn, a similar but not identical event class.



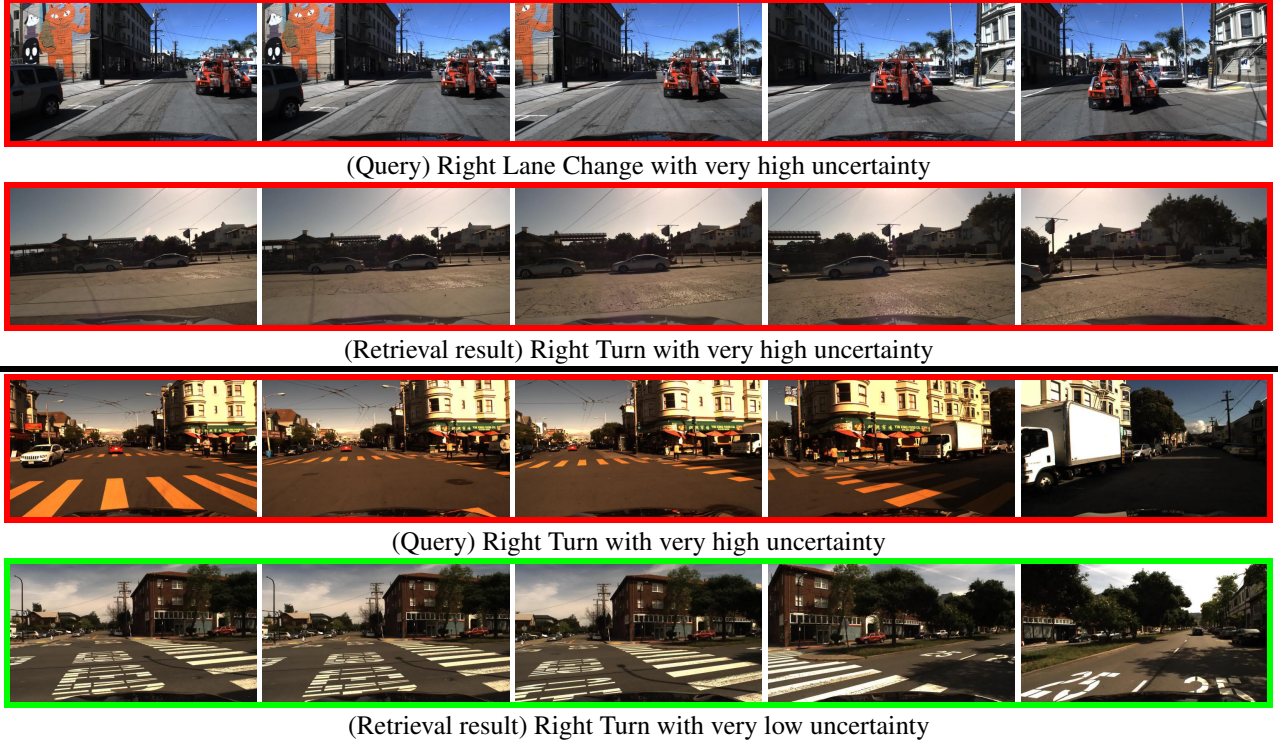


Figure 11: Qualitative evaluation on HDD using goal-oriented events. Every query is followed by the nearest retrieval result. Outline colors emphasize the event uncertainty degree. The first query shows a high uncertainty *right lane change*. The second query shows a *right-turn* maneuver blocked by crossing pedestrian. These images are best viewed in color/screen.

The second query (third row) shows a *right-turn* maneuver where the driver is waiting for crossing pedestrian. The retrieved result (forth row) belongs to the same class but suffers very low uncertainty. We posit the high and low uncertainty are due to pedestrian presence and absence respectively. More visualization using GIFs are available in the supplementary material.

#### 5.4. Discussion

We study uncertainty in visual retrieval systems by introducing an extension to the triplet loss. Our unsupervised formulation models embedding space uncertainty. This improves efficiency of the system and identifies confusing visual examples without raising the computational cost. We evaluate our formulation on multiple domains through three datasets. Real-world noisy datasets highlight the utility of our formulation. Qualitative results emphasize our ability in identifying confusing scenarios. This enables data cleaning and reduces error propagation in safety-critical systems.

One limitation of the proposed formulation is bias against minority classes. It treats minority class training samples as noisy input and attenuates their contribution. Tables 3 and 4 emphasize this phenomenon where performance on the majority and minority classes increases and decreases respec-

tively. Accordingly, micro mAP increases while macro mAP decreases. Thus, this formulation is inadequate for boosting minority classes’ performance in imbalanced datasets.

For image applications, high uncertainty is relatively easy to understand – a favorable quality. Occlusion, inter-class similarity, and multiple distinct instances contribute to visual uncertainty. Unfortunately, this is not the case in video applications, where it’s challenging to explain uncertainty in events with multiple independent agents. Attention model (Xu et al., 2015; Zhou et al., 2016) is one potential extension, which can ground uncertainty in video datasets.

## 6. Conclusion

We propose an unsupervised ranking loss extension to model local noise in embedding space. Our formulation supports various embedding architectures and ranking losses. It quantifies data uncertainty in visual retrieval systems without raising their computational complexity. This raises stability and efficiency for clean and inherently noisy real-world datasets respectively. Qualitative evaluations highlight our approach efficiency identifying confusing visuals. This is a remarkable add-on for safety-critical domains like autonomous navigation.



## References

- Bishop, C. M. et al. *Neural networks for pattern recognition*. Oxford university press, 1995.
- Chen, W., Chen, X., Zhang, J., and Huang, K. Beyond triplet loss: a deep quadruplet network for person re-identification. In *CVPR*, 2017.
- Cheng, D., Gong, Y., Zhou, S., Wang, J., and Zheng, N. Person re-identification by multi-channel parts-based cnn with improved triplet loss function. In *CVPR*, 2016.
- Deng, J., Dong, W., Socher, R., Li, L.-J., Li, K., and Fei-Fei, L. Imagenet: A large-scale hierarchical image database. In *CVPR*, 2009.
- Funahashi, K.-i. and Nakamura, Y. Approximation of dynamical systems by continuous time recurrent neural networks. *Neural networks*, 1993.
- Gal, Y. and Ghahramani, Z. Dropout as a bayesian approximation: Representing model uncertainty in deep learning. In *ICML*, 2016.
- Gal, Y., Islam, R., and Ghahramani, Z. Deep bayesian active learning with image data. *arXiv preprint arXiv:1703.02910*, 2017.
- Hadsell, R., Chopra, S., and LeCun, Y. Dimensionality reduction by learning an invariant mapping. *IEEE*, 2006.
- He, K., Zhang, X., Ren, S., and Sun, J. Deep residual learning for image recognition. In *CVPR*, 2016.
- Hermans, A., Beyer, L., and Leibe, B. In defense of the triplet loss for person re-identification. *arXiv preprint arXiv:1703.07737*, 2017.
- Hochreiter, S. and Schmidhuber, J. Long short-term memory. *Neural computation*, 1997.
- Huang, C., Li, Y., Change Loy, C., and Tang, X. Learning deep representation for imbalanced classification. In *CVPR*, 2016a.
- Huang, C., Loy, C. C., and Tang, X. Local similarity-aware deep feature embedding. In *NIPS*, 2016b.
- Kendall, A. and Gal, Y. What uncertainties do we need in bayesian deep learning for computer vision? In *NIPS*, 2017.
- Le, Q. V., Smola, A. J., and Canu, S. Heteroscedastic gaussian process regression. In *ICML*, 2005.
- Li, Y., Song, Y., and Luo, J. Improving pairwise ranking for multi-label image classification. In *CVPR*, 2017.
- Liao, S., Hu, Y., Zhu, X., and Li, S. Z. Person re-identification by local maximal occurrence representation and metric learning. In *CVPR*, 2015.
- McAllister, R., Gal, Y., Kendall, A., Van Der Wilk, M., Shah, A., Cipolla, R., and Weller, A. V. Concrete problems for autonomous vehicle safety: Advantages of bayesian deep learning. In *International Joint Conferences on Artificial Intelligence, Inc.*, 2017.
- Nair, T., Precup, D., Arnold, D. L., and Arbel, T. Exploring uncertainty measures in deep networks for multiple sclerosis lesion detection and segmentation. In *International Conference on Medical Image Computing and Computer-Assisted Intervention*, 2018.
- Nix, D. A. and Weigend, A. S. Estimating the mean and variance of the target probability distribution. In *Neural Networks, 1994. IEEE World Congress on Computational Intelligence., 1994 IEEE International Conference On*, 1994.
- Ramanishka, V., Chen, Y.-T., Misu, T., and Saenko, K. Toward driving scene understanding: A dataset for learning driver behavior and causal reasoning. In *CVPR*, 2018.
- Ristani, E. and Tomasi, C. Features for multi-target multi-camera tracking and re-identification. *arXiv preprint arXiv:1803.10859*, 2018.
- Sankaranarayanan, S., Alavi, A., Castillo, C., and Chellappa, R. Triplet probabilistic embedding for face verification and clustering. *arXiv preprint arXiv:1604.05417*, 2016.
- Schroff, F., Kalenichenko, D., and Philbin, J. Facenet: A unified embedding for face recognition and clustering. In *CVPR*, 2015.
- Simonyan, K. and Zisserman, A. Two-stream convolutional networks for action recognition in videos. In *NIPS*, 2014.
- Su, C., Zhang, S., Xing, J., Gao, W., and Tian, Q. Deep attributes driven multi-camera person re-identification. In *ECCV*, 2016.
- Sun, Y., Zheng, L., Deng, W., and Wang, S. Svdnet for pedestrian retrieval. *arXiv preprint*, 2017.
- Szegedy, C., Ioffe, S., Vanhoucke, V., and Alemi, A. A. Inception-v4, inception-resnet and the impact of residual connections on learning. In *AAAI*, 2017.
- Taha, A., Chen, Y.-T., Yang, X., Misu, T., and Davis, L. Exploring uncertainty in conditional multi-modal retrieval systems. In *arXiv preprint arXiv:*, 2019.
- Xiao, T., Xia, T., Yang, Y., Huang, C., and Wang, X. Learning from massive noisy labeled data for image classification. In *CVPR*, 2015.

- Xu, K., Ba, J., Kiros, R., Cho, K., Courville, A., Salakhudinov, R., Zemel, R., and Bengio, Y. Show, attend and tell: Neural image caption generation with visual attention. In *ICML*, 2015.
- Zheng, L., Shen, L., Tian, L., Wang, S., Wang, J., and Tian, Q. Scalable person re-identification: A benchmark. In *ICCV*, 2015.
- Zheng, L., Yang, Y., and Hauptmann, A. G. Person re-identification: Past, present and future. *arXiv preprint arXiv:1610.02984*, 2016.
- Zheng, Z., Zheng, L., and Yang, Y. Unlabeled samples generated by gan improve the person re-identification baseline in vitro. *arXiv preprint arXiv:1701.07717*, 2017.
- Zheng, Z., Zheng, L., and Yang, Y. Pedestrian alignment network for large-scale person re-identification. *IEEE Transactions on Circuits and Systems for Video Technology*, 2018.
- Zhou, B., Khosla, A., Lapedriza, A., Oliva, A., and Torralba, A. Learning deep features for discriminative localization. In *CVPR*, 2016.